New Journal of Physics
The open-access journal for physics

# A qubit strongly coupled to a resonant cavity: asymmetry of the spontaneous emission spectrum beyond the rotating wave approximation

**X Cao[1,2,6], J Q You[2,3], H Zheng[4] and F Nori[2,5]**

[1] Department of Physics and Institute of Theoretical Physics and Astrophysics, Xiamen University, Xiamen, 361005, People's Republic of China
[2] Advanced Science Institute, RIKEN, Wako-shi 351-0198, Japan
[3] Department of Physics and State Key Laboratory of Surface Physics, Fudan University, Shanghai 200433, People's Republic of China
[4] Department of Physics, Shanghai Jiao Tong University, Shanghai 200240, People's Republic of China
[5] Physics Department, The University of Michigan, Ann Arbor, MI 48109-1040, USA
E-mail: xfcao@xmu.edu.cn

*New Journal of Physics* **13** (2011) 073002 (21pp)
Received 10 March 2011
Published 5 July 2011
Online at http://www.njp.org/
doi:10.1088/1367-2630/13/7/073002

**Abstract.** We investigate the spontaneous emission (SE) spectrum of a qubit in a lossy resonant cavity. We use neither the rotating-wave approximation nor the Markov approximation. For the weak-coupling case, the SE spectrum of the qubit is a single peak, with its location depending on the spectral density of the qubit environment. Then, the asymmetry (of the location and heights of the two peaks) of the two SE peaks (which are related to the vacuum Rabi splitting) changes as the qubit–cavity coupling increases. Explicitly, for a qubit in a low-frequency intrinsic bath, the height asymmetry of the splitting peaks is enhanced as the qubit–cavity coupling strength increases. However, for a qubit in an Ohmic bath, the height asymmetry of the spectral peaks is inverted compared to the low-frequency bath case. With further increasing the qubit–cavity coupling to the ultra-strong regime, the height asymmetry of the left and right peaks is slightly inverted, which is consistent with the corresponding case of a low-frequency bath. This inversion of the asymmetry arises from the competition between the Ohmic bath and the cavity bath. Therefore, after considering the

[6] Author to whom any correspondence should be addressed.

anti-rotating terms, our results explicitly show how the height asymmetry in the SE spectrum peaks depends on the qubit–cavity coupling and the type of intrinsic noise experienced by the qubit.

**Contents**



## 1. Introduction

Strong and ultra-strong qubit–cavity interactions have been achieved in both cavity quantum electrodynamics (QED) and circuit QED systems (see, e.g., [1–4]). This opens up several new research directions. For example, one can use the cavity as a quantum bus to couple widely separated qubits in a quantum processor [5, 6], as a quantum memory to store quantum information or as a generator and detector of single microwave photons for quantum communications [4].

As a demonstration of strong interaction in cavity QED and circuit QED systems, the vacuum Rabi splitting has been a growing subfield of optics and solid-state physics (see, e.g. [7–10]) after its observation in atomic systems [11]. In 2004, two groups [12, 13] reported the experimental realization of vacuum Rabi splitting in semiconductor systems: a single quantum dot in the spacer of a photonic crystal nanocavity and in a semiconductor microcavity, respectively. In the same year, the experiment [14] observed vacuum Rabi splitting in a superconducting two-level system, playing the role of an artificial atom, coupled to an on-chip cavity consisting of a superconducting transmission line resonator. When the qubit was resonantly coupled to the cavity mode, it was observed [14] that two well-resolved spectral lines were separated by a vacuum Rabi frequency $\nu_{\rm Rabi} \approx 2g$. Except for the asymmetry in the height of the two split energy-peaks (e.g. [14]), the data are in agreement with the transmission spectrum numerically calculated using the rotating wave approximation (RWA). When considering the vacuum Rabi splitting for *strong* qubit–cavity coupling, the anti-rotating terms should be taken into account, and this might explain the observed [14] *asymmetric* SE spectrum.

### *1.1. Anti-rotating terms are important for strong coupling QED*

The effect of anti-rotating terms on the atomic spectra has been noted earlier [15–17]. More recently, in the *ultra-strong coupling* regime, the anti-rotating coupling terms of the intrinsic bath to the qubit became more important [18–21]. As a consequence of the anti-rotating terms in the Hamiltonian of cavity QED and circuit QED, even the ground state of the system contains a finite number of virtual photons. Theoretical research [22, 23] revealed that these virtual photons can be released by a nonadiabatic manipulation, where the Rabi frequency $g(t)$ is modulated in time at frequencies comparable to or higher than the qubit transition frequency. This phenomenon, called 'emission of the quantum vacuum radiation', would be completely absent if these anti-rotating terms are neglected. The energy shift of the qubit in its intrinsic bath has been studied in [24] using the full description (i.e. non-Markov and without RWA) and it was found that the deviation from the previous approximate result already amounts to $\sim$5% for $g/\Delta \sim 0.1$ (where $g$ is the qubit–cavity coupling strength and $\Delta$ is the energy spacing of the qubit).

In doped semiconductor quantum wells embedded in a microcavity, considering the anti-rotating coupling of the intracavity photonic mode and the electronic polarization mode, but using RWA in the coupling to their respective environments, it was found [25] that for a coherent photonic input, signatures of the ultra-strong coupling have been identified in the asymmetric and peculiar anti-crossing of the polaritonic eigenmodes. From the descriptions given above, it can be seen that as $g/\Delta$ increases to the ultra-strong coupling limit, the anti-rotating terms that were negligible before become more relevant and will lead to a profound modification in the nature of the quantum state of the qubit system.

### *1.2. The asymmetry of the two splitting Rabi peaks beyond the rotating wave approximation (RWA) approximation*

In this paper, we study the spontaneous emission (SE) spectrum of a qubit in a cavity. Our calculations include *two kinds of anti-rotating terms*: one from the intrinsic qubit bath and the other from the cavity bath. Our method is a powerful tool for investigating various kinds of qubit–environment interaction beyond the RWA and the Markov approximation. Comparing the case of a qubit in an Ohmic bath with the case of a qubit in a low-frequency bath, we find that in the case of a qubit in a low-frequency bath, as the qubit–cavity coupling strength increases, the height asymmetry of two splitting peaks is enhanced. However, in the case of a qubit in an Ohmic bath, the height asymmetry of the spectral peaks is inverted from the corresponding case of a low-frequency bath when the qubit is strongly coupled to the cavity; with further increasing the qubit–cavity coupling to the ultra-strong regime, the height asymmetry of the left and right peaks is slightly inverted, which is consistent with the corresponding case of a low-frequency bath. Since experiments reported that *a superconducting qubit intrinsic bath is mainly due to low-frequency noise, our results are consistent with experimental data* [14] using a superconducting qubit. We also investigate the dependence of the SE spectrum on the strength of the qubit–cavity coupling and the quality factor $Q$ of the cavity in either an Ohmic or a low-frequency intrinsic qubit bath. Furthermore, we identify the contributions to asymmetry from the baths, and clarify the reason for the different kinds of peak asymmetry.

SE spectra under strong- and ultra-strong couplings are, for the most part, sharp doublets, with each peak well localized, isolated from the other. The main factors that determine peak properties, e.g. location and height, are the anti-rotating terms and the local (at the peak

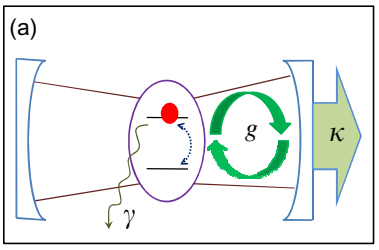


**Figure 1.** Schematic diagram of a two-level system or qubit with dissipation rate $\gamma$, which is coupled to a cavity with loss rate $\kappa$ by the qubit–cavity coupling strength $g$.

resonance) bath coupling strength and density of states. Thus, one can explain many of the reported results by performing a calculation for each peak, but using the local properties of the bath and involving the anti-rotating terms. In particular, the observed different behavior for the low-frequency versus Ohmic bath are readily explained in this way. Our results directly indicate that in the strong coupling regime, the SE spectrum is deeply influenced by the anti-rotating terms and the type of intrinsic noise experienced by the qubit.

## 2. Beyond the RWA

By using a cavity to confine the electromagnetic field, the strength of the qubit–cavity interaction can be increased by several orders of magnitude to the regime of strong or even ultra-strong coupling [26]. The strong-coupling regime for cavity QED has been reached for superconducting qubits in circuit resonators (i.e. on-chip cavities) and quantum dots in photonic-crystal nanocavities. Recently, the ultra-strong coupling regime was achieved for a superconducting qubit in an on-chip cavity [2].

Although the coupling of the qubit to the cavity is much stronger than the coupling of the qubit to its intrinsic environment, the parameters in [14] show that both the decay rate of the cavity photon ($\kappa/2\pi \approx 0.8\,\mathrm{MHz}$) and the qubit decoherence rate ($\gamma/2\pi \approx 0.7\,\mathrm{MHz}$) are comparable. Therefore, we model the environment of the qubit in a cavity using two bosonic baths: one, called the 'intrinsic bath' of the qubit and represented by operators $a_{k,1}$ and $a_{k,1}^{\dagger}$, is related to the relaxation of the qubit induced by its intrinsic environment; and the other, denoted as 'cavity bath' of the qubit and represented by the operators $a_{k,2}^{\dagger}$ and $a_{k,2}$, involves the relaxation of the qubit caused by photons in the cavity.

Figure 1 schematically shows the model considered here. For the intrinsic qubit bath, a broad frequency spectrum (e.g. either an Ohmic or a low-frequency spectrum) can be used to characterize it. For the cavity bath, because of the cavity leakage, it can be described by a Lorentzian spectrum with a central frequency, i.e. a single-mode cavity with its frequency broadened by the cavity leakage.

The Hamiltonian can be written (throughout this paper, we choose $\hbar = 1$) [25] as

$$H = \frac{1}{2}\Delta\sigma_z + \sum_{k,i} \omega_{k,1} a_{k,i}^{\dagger} a_{k,i} + \sum_{k,i} g_{k,i}(a_{k,i}^{\dagger} + a_{k,i})\sigma_x, \tag{1}$$

where $\Delta$ is the qubit energy spacing, $i = 1$ for the intrinsic bath and $i = 2$ for the cavity bath. The baths experienced by the qubit can be characterized by a spectral density $J_i(\omega) = \sum_k g_{k,i}^2 \delta(\omega - \omega_{k,i})$.

To deal with the anti-rotating terms in equation (1), we apply two unitary transformations to the Hamiltonian $H$ as $H' = \exp(S)H\exp(-S)$ (see appendix A). The transformed Hamiltonian $H'$ can be written as

$$H' \approx \frac{1}{2}\eta\,\Delta\sigma_z + \sum_{k,i}\omega_{k,i}a^{\dagger}_{k,i}a_{k,i} + \sum_{k,i}\tilde{g}_{k,i}(a^{\dagger}_{k,i}\sigma_- + a_{k,i}\sigma_+), \tag{2}$$

where

$$\tilde{g}_{k,i} = \left(\frac{2\eta_i\Delta}{\omega_{k,i}+\eta_i\Delta}\right)g_{k,i}, \tag{3}$$

$$\eta = \eta_1\eta_2, \tag{4}$$

with

$$\eta_i = \exp\left(-\sum_k \frac{2g^2_{k,i}}{\omega^2_{k,i}}\,\xi^2_{k,i}\right). \tag{5}$$

Using $J_i(\omega) = \sum_k g^2_{k,i}\delta(\omega-\omega_{k,i})$, one can derive that $\eta_i$ is determined self-consistently by the equation

$$\log\eta_i + \int_0^{\infty}\frac{2J_i(\omega)\mathrm{d}\omega}{(\omega+\eta_i\,\Delta)^2} = 0. \tag{6}$$

Here we re-emphasize that the transformed Hamiltonian contains the zero-boson transition in $\eta$ and the terms of single-boson transition in $H'_1$, whose contributions to the physical quantities are $\mathcal{O}(g^2_{k,i})$, and drops the multiboson nondiagonal transition $(a^{\dagger}_{k,i}a^{\dagger}_{k',i}, a_{k,i}a_{k',i})$, whose contributions to the physical quantities are $\mathcal{O}(g^4_{k,1})$, $\mathcal{O}(g^4_{k,2})$ or $\mathcal{O}(g^2_{k,1}g^2_{k,2})$. Now the transformed Hamiltonian (2) has the same form as the Hamiltonian under the RWA, but its parameters have been renormalized to include the effects of the anti-rotating terms related to the intrinsic and cavity baths of the qubit.

From the transformed Hamiltonian $H'$, one can see that, based on energy conservation, the ground state of the transformed Hamiltonian $H'$ is

$$|g'\rangle = |\downarrow\rangle\otimes\prod_k|0_{k,1},0_{k,2}\rangle, \tag{7}$$

($\sigma_z|\downarrow\rangle = -|\downarrow\rangle$) and the corresponding ground-state energy is $-\eta\Delta/2$. Therefore, the ground state of the original Hamiltonian $H$ is given by

$$|g\rangle = \exp(-S)\,|g'\rangle, \tag{8}$$

which is a dressed state of the qubit and its baths due to the anti-rotating terms [22, 23]. In this paper, we choose the initial excited state as

$$|\psi(0)\rangle = \exp(-S)\,|\uparrow\rangle\otimes\prod_k|0_{k,1},0_{k,2}\rangle, \tag{9}$$

which can be achieved by $\sigma_x|g\rangle$. It is obvious that this initial state is also a dressed state.

A qubit can experience different types of intrinsic baths. The most commonly used bath is the photon or phonon bath, which can be described by an Ohmic spectrum. However, for many solid-state qubits (e.g. superconducting qubits), the dominant dissipation is due to two-level

fluctuators, which behave like a low-frequency bath [27]. Here we consider either an Ohmic or a low-frequency intrinsic bath. The Ohmic bath with the Drude cutoff is given by

$$J_1^{\rm Ohm}(\omega) = \frac{2\,\alpha_{\rm Ohm}\omega}{1+(\omega/\omega_{\rm Ohm})^2}, \tag{10}$$

where $\omega_{\rm Ohm}$ is the high-frequency cutoff and $\alpha_{\rm Ohm}$ a dimensionless parameter characterizing the coupling strength between the qubit and its intrinsic bath. Here the low-frequency bath is written as

$$J_1^{\rm low}(\omega) = \frac{2\alpha_{\rm low}\omega}{(\omega/\Delta)^2+(\omega_{\rm low}/\Delta)^2}, \tag{11}$$

where $\omega_{\rm low}$ is a characteristic frequency lower than the qubit energy spacing $\Delta$ of the qubit, and $\alpha_{\rm low}$ is the dimensionless coupling strength between the qubit and its intrinsic bath. If $\omega \geqslant \omega_{\rm low}$, $J_1^{\rm low}(\omega) \sim 1/\omega$, corresponding to $1/f$ noise.

For a lossy cavity, the bath can be described by a Lorentzian spectral density with a central frequency [28]:

$$J_2(\omega) = \frac{g^2\lambda}{\pi[(\omega-\omega_{\rm cav})^2+\lambda^2]}, \tag{12}$$

which corresponds to a single-mode cavity, with its frequency broadened by the cavity loss. In equation (12), $\lambda$ is the frequency width of the cavity bath density spectrum, $\omega_{\rm cav}$ is the central frequency of the cavity mode, and $g$ denotes the coupling strength between the qubit and the cavity. Also, the parameter $\lambda$ is related to the cavity bath correlation time and $\omega_{\rm cav}/\lambda$ is the quality factor $Q$ of the cavity.

Below we will solve the equation of motion for the density matrix in Hamiltonian (1) and obtain the qubit SE spectrum.

### *2.1. Equation of motion for the density matrix*

The equation of motion for the density matrix $\rho_{SB}$ for the whole system, i.e. the qubit system ($S$) and the bath ($B$), is given by

$$\frac{\rm d}{{\rm d}t}\rho_{SB}(t) = -{\rm i}[H, \rho_{SB}(t)]. \tag{13}$$

After the unitary transformations, we have

$$\frac{\rm d}{{\rm d}t}\rho'_{SB}(t) = -{\rm i}[H', \rho'_{SB}(t)], \tag{14}$$

where $\rho'_{SB} = \exp(S)\rho_{SB}\exp(-S)$ is the density matrix of the whole system in the Schrödinger picture with the transformed Hamiltonian $H'$ (i.e. equation (2)). In the interaction picture, the transformed Hamiltonian $H'$ is written as

$$V'_{\rm I}(t) = \sum_{k,i} \tilde{g}_{k,i} a^\dagger_{k,i}\sigma_- \exp[{\rm i}(\omega_{k,i}-\eta\,\Delta)t] + {\rm h.c.} \tag{15}$$

The equation of motion for the density matrix $\rho'^{\rm I}_{SB}(t)$ of the whole system ($S$+$B$) can be written as

$$\frac{\rm d}{{\rm d}t}\rho'^{\rm I}_{SB}(t) = -{\rm i}[V'_{\rm I}(t), \rho'_{SB}(0)] - \int_0^t [V'_{\rm I}(t), [V'_{\rm I}(t'), \rho'^{\rm I}_{SB}(t')]]\,{\rm d}t'. \tag{16}$$

Under the Born approximation [29] and tracing over the degrees of freedom of the two baths, one obtains [30]

$$\frac{\mathrm{d}}{\mathrm{d}t}\rho_S'^{\mathrm{I}}(t) = -\mathrm{i}\mathrm{Tr}_B[V_{\mathrm{I}}'(t), \rho_S'(0)\otimes\rho_B'(0)] - \mathrm{Tr}_B\int_0^t [V_{\mathrm{I}}'(t), [V_{\mathrm{I}}'(t'), \rho_S'^{\mathrm{I}}(t')\otimes\rho_B(0)]]\,\mathrm{d}t', \tag{17}$$

where $\rho'^{\mathrm{I}}_S(t) = \mathrm{Tr}_B[\rho'^{\mathrm{I}}_{SB}(t)]$. Then, substituting $V_{\mathrm{I}}'(t)$ (15) into equation (17), we have

$$\frac{\mathrm{d}}{\mathrm{d}t}\rho_S'^{\mathrm{I}}(t) = -\sum_{k,i}\tilde{g}_{k,i}^2\int_0^t f(t')\exp[\mathrm{i}(\omega_{k,i}-\eta\,\Delta)(t-t')]\mathrm{d}t' - \mathrm{h.c.},$$

where

$$f(t') = n_{k,i}[\sigma_-\sigma_+\rho_S'^{\mathrm{I}}(t') - \sigma_+\rho_S'^{\mathrm{I}}(t')\sigma_-] + (n_{k,i}+1)[\rho_S'^{\mathrm{I}}(t')\sigma_+\sigma_- - \sigma_-\rho_S'^{\mathrm{I}}(t')\sigma_+], \tag{18}$$

and $n_{k,i}$ is the thermal average boson number at mode $k$ in the bath $i$. In the right-hand side of equation (18), the terms related to $n_{k,i}$ and $n_{k,i}+1$ describe, respectively, the decay and excitation processes, with the rates depending on the temperature. Here, for simplicity, we study the zero-temperature case with $n_{k,i}=0$, i.e. only the spontaneous decay occurs, which corresponds to a purely dissipative process. Therefore, the reduced density matrix $\rho_S'(t)$ of the qubit in the Schrödinger picture is obtained as (for the details, see appendix B)

$$\begin{aligned}\rho_S'(t) &= \exp(\mathrm{i}\eta\Delta\sigma_z t/2)\rho_S'^{\mathrm{I}}(t)\exp(\mathrm{i}\eta\Delta\sigma_z t/2)\\ &= \begin{pmatrix} \mathcal{L}^{-1}\left[\frac{\rho_{22}'(0)}{p+A_++A_-}\right] & \mathcal{L}^{-1}\left[\frac{\rho_{21}'(0)}{p+A_+}\right]\mathrm{e}^{-\mathrm{i}t\Delta\eta} \\ \mathcal{L}^{-1}\left[\frac{\rho_{12}'(0)}{p+A_-}\right]\mathrm{e}^{\mathrm{i}t\Delta\eta} & \mathcal{L}^{-1}\left[\frac{\rho_{22}'(0)}{p} - \frac{\rho_{22}'(0)}{p+A_++A_-} + \frac{\rho_{11}'(0)}{p}\right]\end{pmatrix},\end{aligned} \tag{19}$$

where $\mathcal{L}^{-1}$ represents the inverse Laplace transform, $p$ the complex argument and $A_\pm = \sum_{k,i}^2 \tilde{g}_{k,i}^2/[p\pm\mathrm{i}(\omega_{k,i}-\eta\Delta)]$.

### 2.2. Derivation of the spontaneous emission (SE) spectrum

When measured by an ideal system with negligible bandwidth, the SE spectrum can be given by [31]

$$P(\omega) \propto \int_0^\infty \mathrm{d}t\int_0^\infty \mathrm{d}t'\exp[-\mathrm{i}\omega(t-t')]C(t,t'), \tag{20}$$

with the two-time correlation function

$$\begin{aligned}C(t,t') &= \langle\sigma_+(t)\sigma_-(t')\rangle\\ &= \langle\psi(0)|\,\sigma_+(t)\sigma_-(t')|\psi(0)\rangle.\end{aligned} \tag{21}$$

Since we have obtained the density matrix $\rho_S'(t)$ in the above derivation, we now solve the two-time correlation function in the transformed Hamiltonian

$$C(t,t') = \langle\psi'(0)|\mathrm{e}^{\mathrm{i}H't}\sigma_+\mathrm{e}^{-\mathrm{i}H't}\mathrm{e}^{\mathrm{i}H't'}\sigma_-\mathrm{e}^{-\mathrm{i}H't'}|\psi'(0)\rangle, \tag{22}$$

with $|\psi'(0)\rangle = \exp(S)|\psi(0)\rangle$.

For a qubit state specified by a density matrix $\rho(t)$, we can formulate the expectation values of $\sigma_+(t)$, $\sigma_-(t)$ and $\sigma_+(t)\sigma_-(t)$ by the matrix elements $\langle\sigma_+(t)\rangle = \langle\sigma_-(t)\rangle^* = \rho_{21}(t)$ and

$C(t,t)=\rho_{11}(t)$. According to the quantum regression theorem [31], the correlation function becomes

$$C(t,t+\tau)_{H'}=\mathcal{L}^{-1}\left(\frac{1}{p+A_+}\right)_{\tau}\mathrm{e}^{-\mathrm{i}\Delta\eta\tau}\rho'_{11}(t). \tag{23}$$

Then, the initial state in the transformed Hamiltonian (2) is $|\psi'(0)\rangle=|\uparrow\rangle\otimes\prod_k\left|0_{k,1},0_{k,2}\right\rangle$, i.e. $\rho'_{11}(0)=1$. In this paper, we only focus on the single-particle excitation case (either the baths or the system). When considering the case of the multiple-particle excitation, the two-photon term should be included [32]. Therefore, from equation (B.12) in appendix B, the dynamical evolution of $\rho'_{11}$ is expressed as

$$\rho'_{11}(t)=\mathcal{L}^{-1}\left(\frac{1}{p+A_++A_-}\right)_t. \tag{24}$$

From appendix C, we have [33]

$$\mathcal{L}^{-1}\left(\frac{1}{p+A_++A_-}\right)_t=\mathcal{L}^{-1}\left(\frac{1}{p+A_+}\right)_t\times\mathcal{L}^{-1}\left(\frac{1}{p+A_-}\right)_t, \tag{25}$$

where $\mathcal{L}^{-1}(\frac{1}{p+A_+})$ and $\mathcal{L}^{-1}(\frac{1}{p+A_-})$ are conjugate quantities. Then, the two-time correlation function for any $t$ and $t'$ becomes

$$C(t,t')_{H'}=\mathcal{L}^{-1}\left(\frac{1}{p+A_+}\right)_t\mathrm{e}^{-\mathrm{i}\Delta\eta t}\mathcal{L}^{-1}\left(\frac{1}{p+A_-}\right)_{t'}\mathrm{e}^{-\mathrm{i}\Delta\eta t'}. \tag{26}$$

Finally, using the Wiener–Khinchin theorem, the SE spectrum is given by

$$\begin{aligned}P(\omega)&\propto\int_0^\infty\mathrm{d}t\int_0^\infty\mathrm{d}t'\exp[-\mathrm{i}\omega(t-t')]C(t,t')\\&=\left|\mathcal{F}\left[\mathcal{L}^{-1}\left(\frac{1}{p+A_+}\right)\mathrm{e}^{-\mathrm{i}\Delta\eta\tau}\right]\right|^2\\&=\frac{1}{[\omega-\Delta\eta-R(\omega)]^2+\Gamma(\omega)^2},\end{aligned} \tag{27}$$

where $\mathcal{F}$ is the Fourier transform.

## 3. Dependence of the SE spectrum on the baths

We will show the SE spectrum of the qubit in resonance with the cavity central frequency ($\Delta=\omega_{\mathrm{cav}}$) as a function of the microwave probe frequency for three cases: weak, strong and ultra-strong qubit–cavity couplings.

*Weak coupling* means that the qubit–cavity coupling strength $g$ is less than the sum of the dissipation rate of the qubit and cavity. The dissipation rate of the qubit due to its intrinsic bath is approximately denoted by $\Gamma_{\mathrm{qb}}$, which is approximated as $\alpha_{\mathrm{Ohm}}\Delta$ or $\alpha_{\mathrm{low}}\Delta$. Also, the dissipation rate due to the cavity bath can be approximately equal to the spectrum width of the cavity spectral density $\lambda$. Thus, weak coupling can be expressed as $g<(\Gamma_{\mathrm{qb}}+\lambda)$.

*Strong coupling* means that the qubit–cavity coupling strength $g$ is larger than the sum of the dissipation rate of the qubit and the cavity: $g>(\Gamma_{\mathrm{qb}}+\lambda)$, but it is typically two orders of magnitude smaller than the qubit energy spacing $\Delta$ and the cavity frequency $\omega_{\mathrm{cav}}$, i.e. $g\sim10^{-2}\Delta$, such as the case in [14].

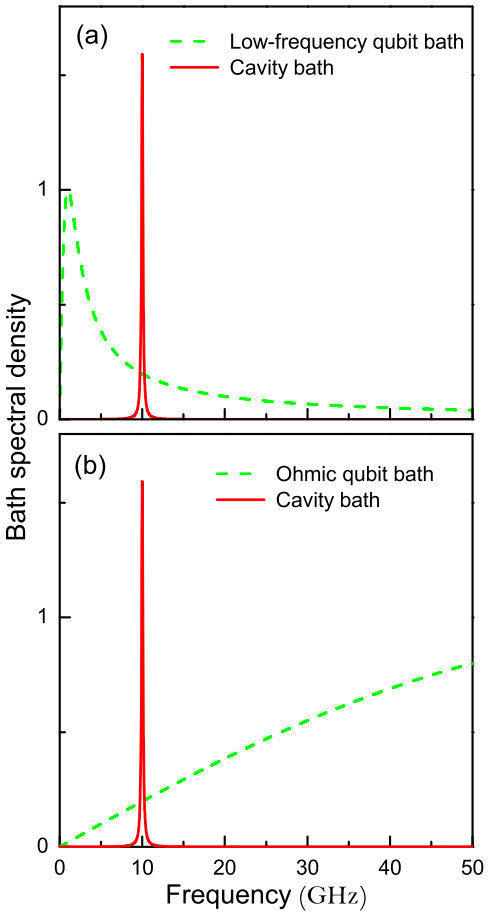


**Figure 2.** The spectrum density of the qubit environment. (a) Lorentzian cavity bath and low-frequency intrinsic bath of the qubit. (b) Lorentzian cavity bath and Ohmic intrinsic bath of the qubit. From (a) and (b), it is evident that the dominant regimes of the low-frequency and Ohmic qubit bath spectral densities are different.

*Ultra-strong coupling* means that the qubit–cavity coupling $g$ is a significant fraction of the transition frequency $\Delta$ (e.g. $g \gtrsim 0.1\Delta$). This case extends to the fine-structure limit for the maximal value of an electric–dipole coupling.

The properties of the bath, especially the local properties (bath coupling strength and density of states) at the resonant peak, play an important role in determining the energy-shift direction and the asymmetry of the SE spectrum [34, 35]. In figure 2, we show the spectral densities of the qubit intrinsic bath and the cavity bath. For the qubit intrinsic bath, both a low-frequency bath and an Ohmic bath are considered. The spectral density of the cavity bath is symmetric about the central frequency $\omega_{\rm cav}$ of the cavity.

Considering the experimental parameters [14, 36], we assume the qubit energy spacing to be $\Delta = 10\,\mathrm{GHz}$. The dimensionless coupling strength $\alpha$ between the qubit and its intrinsic bath (either Ohmic or low-frequency bath) is fixed at $\alpha = 10^{-4}$, which implies that the decay rate of the intrinsic bath is $\Gamma_{\rm qb} \sim 1\,\mathrm{MHz}$.

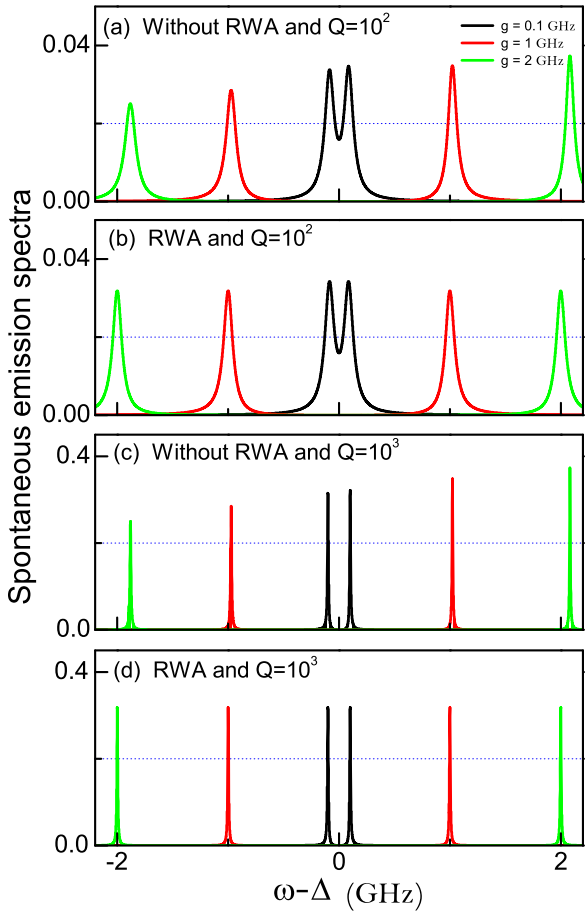


**Figure 3.** The SE spectra of the qubit only in the cavity bath (symmetric spectral density). Panels (a) and (c) show the results without RWA with $Q = 10^2$ and $Q = 10^3$, respectively. Panels (b) and (d) show the results of the RWA with $Q = 10^2$ and $Q = 10^3$. To see the height asymmetry of two peaks clearly, horizontal grid lines are plotted as a reference. Note that in (a) and (c), the two peaks of the SE spectrum present an obvious height and position asymmetry (about $\omega = \Delta$) in the ultra-strong qubit–cavity coupling.

### *3.1. Effect of the cavity bath on the SE spectrum*

To illustrate the effect of the cavity bath with a symmetric spectral density, in figure 3 we show the qubit SE spectrum when only the cavity bath is present. To enhance these features further, we choose the low quality factors $Q = 10^2$ and $Q = 10^3$, and plot the SE spectra in figures 3(a) and (c) for strong ($g = 10^2$ MHz) and ultra-strong ($g = 10^3$, $2 \times 10^3$ MHz) qubit–cavity couplings. For comparison, the results obtained under RWA are given in figures 3(b) and (d). In the case of strong qubit–cavity coupling, the two peaks of the vacuum Rabi splitting are nearly symmetric about $\omega = \Delta$, almost coinciding with the results obtained under RWA. When the qubit–cavity coupling increases, the height and position asymmetry (about the qubit energy spacing $\Delta$) of the two peaks becomes more apparent, in sharp contrast to the symmetric SE peaks obtained under RWA (see figures 3(a)–(d)).

If RWA is used, the qubit–cavity coupling term $\sum_k g_{k,2}(a^\dagger_{k,2} + a_{k,2})(\sigma_+ + \sigma_-)$ in the Hamiltonian $H$ becomes $\sum_k g_{k,2}(a^\dagger_{k,2}\sigma_- + a_{k,2}\sigma_+)$. The energy spectral densities in the regions lower and higher than the central frequency of the cavity $\omega_{\rm cav}$ (related to absorbing and emitting a single photon in the cavity) are identical. Therefore, when the qubit energy spacing $\Delta$ is resonant with the cavity central frequency $\omega_{\rm cav}$, the coupling strength for the absorption and emission processes is symmetric about the qubit energy spacing $\Delta$.

While taking into account the anti-rotating terms, the coupling term becomes $\sum_k \tilde{g}_{k,2}(a^\dagger_{k,2}\sigma_- + a_{k,2}\sigma_+)$ in the transformed Hamiltonian $H'$, with a renormalized coupling strength $\tilde{g}_{k,2} = 2\eta_2\,\Delta g_{k,2}/(\omega_{k,2} + \eta_2\Delta)$. Obviously, *the renormalized coupling strength* $\tilde{g}_{k,2}$ *induces the SE spectral asymmetry*: for a symmetric spectral density of the cavity bath, in the region $\omega_{k,2} < \Delta$, due to $2\eta_2\Delta/(\omega_{k,2} + \eta_2\,\Delta) > 1$, the renormalized interaction $\tilde{g}_{k,2}$ is *larger* than $g_{k,2}$. However, in the region $\omega_{k,2} > \Delta$, owing to $2\eta_2\,\Delta/(\omega_{k,2} + \eta_2\Delta) < 1$, the effective coupling strength $\tilde{g}_{k,2}$ is *smaller* than $g_{k,2}$.

These results (with and without the RWA) indicate that the RWA cannot be used in the range of ultra-strong qubit–cavity coupling. The general tendency observed here is that *the RWA overestimates the frequency shift in the low-energy regime* $\omega \sim -g$, *while it underestimates the frequency shift in the higher-energy regime* $\omega \sim g$. Our results are consistent with the results in [20].

### *3.2. Combined effect of both intrinsic and cavity baths on the SE spectrum*

Although a high $Q$ seems plausible for minimizing the loss of the cavity, it limits the measurement speed. Here, we consider a cavity with the quality factor [8, 14] $Q = 10^4$ in the presence of a qubit (see figure 4). We also plot the SE spectrum for $Q = 10^3$ in figure 5, and show how the quality factor affects the results. If $Q = 10^4$, the dissipation rate of the cavity bath is about 1 MHz (of the same order of magnitude as the bath dissipation rate). Figures 4(a) and (b) show the spectra of the qubit coupled with a low-frequency and an Ohmic intrinsic bath, respectively. From figure 4(a), we see that in the case of weak qubit–cavity coupling ($g = 10^{-5}\Delta = 0.1$ MHz), the SE spectrum is a single peak with the central frequency larger than the energy spacing $\Delta$ of the bare qubit, which corresponds to a blue shift [18]. In the case of *strong* qubit–cavity coupling, $g = 2 \times 10^{-2}\Delta = 2 \times 10^2$ MHz, the SE spectrum shows the vacuum Rabi splitting, with the two height asymmetric peaks, just as shown in [14]. With further increasing the qubit–cavity coupling to the ultra-strong regime (e.g. $g = 10^{-1}\Delta = 1$ GHz), not only the height of the SE peaks but also their positions demonstrate a strong asymmetry about $\omega = \Delta$.

Figure 4(b) shows the SE spectrum of a qubit in the Ohmic intrinsic bath. For a weak qubit–cavity coupling, the central frequency of the SE spectrum shifts to an energy slightly lower than the energy spacing $\Delta$ of the bare qubit (with the peak located at $\omega - \Delta \sim -2.9$ MHz), which corresponds to a red shift. This energy-shift direction is opposite to the case when the qubit is in a low-frequency intrinsic bath (see figure 4(a)). For a strong qubit–cavity coupling, the two SE peaks also show a weak asymmetry, with the left peak higher than the right peak. This peak asymmetry is inverted from the corresponding case in figure 4(a). As the qubit–cavity coupling increases to the ultra-strong regime, the height asymmetry of the left and right SE spectrum is inverted (see figure 4(b)). This inversion of the asymmetry of SE spectra shows the competition between the Ohmic bath and the cavity bath. The SE spectra of the qubit in a cavity with the quality factor $Q = 10^3$ are shown in figure 5, which present nearly the same features as

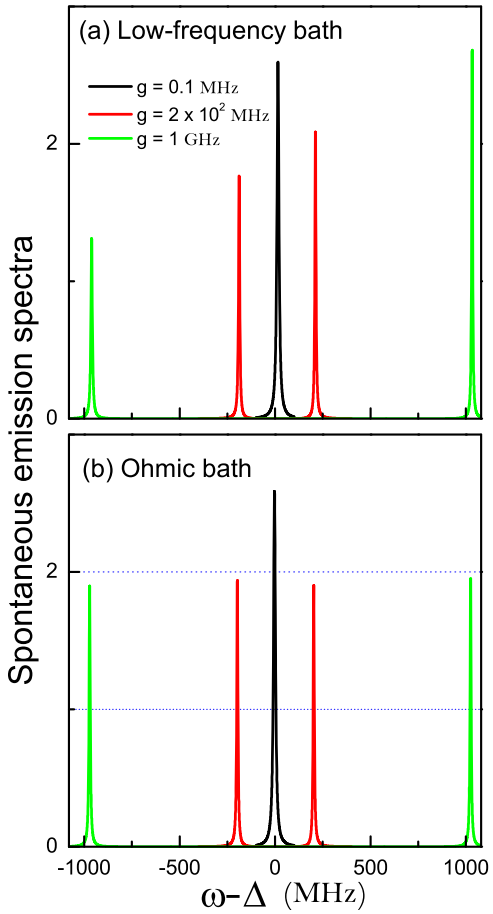


**Figure 4.** The SE spectra of the qubit in resonance with the central frequency of the cavity for weak, strong and ultra-strong qubit–cavity interactions. The quality factor of the cavity is $Q = 10^4$. (a) Coupling strength to the low-frequency intrinsic bath of the qubit $\alpha_{\rm low} = 10^{-4}$; (b) coupling strength to the Ohmic intrinsic bath of the qubit $\alpha_{\rm Ohm} = 10^{-4}$. To see the height asymmetry of the peaks clearly, the horizontal grid lines are plotted as a reference. Note that panel (a) demonstrates an obvious height asymmetry in the case of strong and ultra-strong qubit–cavity coupling and the asymmetry increases as the qubit–cavity coupling grows. Panel (b) shows the very small inverted height asymmetry of two peaks from panel (a) in the strong qubit–cavity coupling case, but as the qubit–cavity coupling increases to the ultra-strong regime, the height asymmetry of the right and left spectral peaks becomes inverted.

those in figure 4, in addition to the broader SE peaks in figure 5. This is because of an increased dissipation rate of the qubit induced by a larger cavity dissipation rate. These results are briefly summarized in table 1.

Figures 4 and 5 show that the two SE peaks of the qubit in both low-frequency and Ohmic intrinsic baths show very different behavior; the right SE peak is higher than the left SE peak in both strong and ultra-strong qubit–cavity coupling regimes, whereas the right SE peak is lower than the left SE peak in the strong qubit–cavity coupling regime; in the ultra-strong qubit–cavity

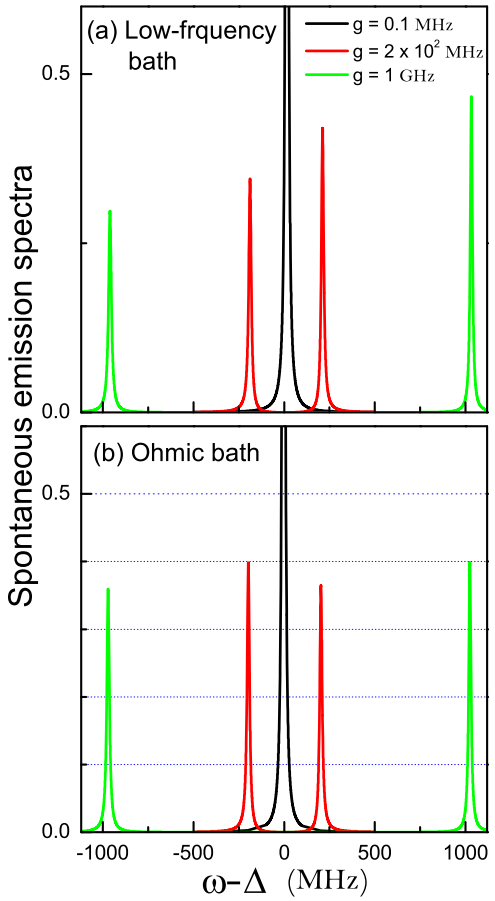


**Figure 5.** The SE spectra of the qubit in resonance with the central frequency of the cavity for weak, strong and ultra-strong qubit–cavity interactions. The quality factor of the cavity is $Q = 10^3$. (a) Coupling strength to the low-frequency intrinsic bath of the qubit $\alpha_{\rm low} = 10^{-4}$; (b) coupling strength to the Ohmic intrinsic bath of the qubit $\alpha_{\rm Ohm} = 10^{-4}$. To see the height asymmetry of the peaks clearly, the horizontal grid lines are plotted as a reference. Note that panel (a) demonstrates obvious height asymmetry in the case of strong and ultra-strong qubit–cavity coupling and the asymmetry increases as the qubit–cavity coupling grows. Panel (b) shows inverted height asymmetry of two peaks from panel (a) in the strong qubit–cavity coupling case, but as the qubit–cavity coupling increases to the ultra-strong regime, the height asymmetry of the right and left spectral peaks is inverted.

coupling regime, the left SE peak is slightly lower than the right peak. In subsection 3.1, we have shown that in the Lorentzian cavity bath, the interaction in the region $\omega_{k,2} < \Delta$, due to the anti-rotating terms, is increased, and yet the coupling in the opposite direction is reduced. In the low-frequency intrinsic bath, dissipation of the qubit energy primarily occurs for energies lower than the energy spacing $\Delta$. Therefore, the energy shift and the asymmetry in the SE spectrum are constructively strengthened when both low-frequency and cavity baths coexist. However, energy dissipation in the Ohmic intrinsic bath mainly occurs for energies higher than the energy

**Table 1.** A summary of our main results for the SE spectra in the case of strong and ultra-strong qubit–cavity couplings. The spectra with height asymmetric peaks and very asymmetric peaks are denoted by AS and VAS. The asterisks indicate the inverted peak height asymmetry from the AS in the low-frequency bath case. These results are described in detail in the main text.

| Bath | Cavity | Qubit–cavity coupling | | |
|---|---|---|---|---|
| | Quality factor | Weak | Strong | Ultra-strong |
| Low-frequency | High $Q$ | Single peak | AS | VAS |
| | Low $Q$ | Single peak | AS | VAS |
| Ohmic | High $Q$ | Single peak | AS* | AS |
| | Low $Q$ | Single peak | AS* | AS |

spacing $\Delta$, and this energy regime is opposite to that for the cavity bath. Therefore, the effects on the SE spectrum produced by the Ohmic intrinsic bath and the cavity bath compete with each other.

Therefore, the different asymmetric behavior of the SE spectrum of the qubit in the low-frequency and Ohmic baths may be used to identify the intrinsic noise of the qubit. In the experiment in [14], the height asymmetric SE spectrum of the qubit in the strong qubit–cavity coupling regime shows that the right SE peak is higher than the left SE peak. This reveals that *the low-frequency intrinsic noise is dominant* in the superconducting qubit in [14].

## 4. Conclusion

In conclusion, we have discussed the SE spectrum of a qubit in the environment described by two baths: an intrinsic bath and a cavity bath. We only considered that the central frequency of the cavity mode is resonant with the qubit energy spacing ($\omega_{cav} = \Delta$). We analyzed in detail the qubit's SE spectrum in the weak, strong and ultra-strong coupling regimes, and compare the SE spectra in two kinds of qubit baths: low-frequency and Ohmic baths. In the low-frequency bath, the height asymmetry of the vacuum Rabi splitting peaks increases as the coupling strength grows. However, for the Ohmic bath, the height asymmetry of the SE spectrum is reduced and the height asymmetry of the left and right peaks is inverted, when the coupling strength is increased. Our results show that for strong qubit–cavity coupling, the combination of the anti-rotating terms and the properties of the baths can cause different types of asymmetries of the splitting peaks in the SE spectrum.

## Acknowledgments

We are grateful to Adam Miranowicz for his helpful comments. FN acknowledges partial support from DARPA, AFOSR, the Laboratory of Physical Sciences, the National Security Agency, the Army Research Office, National Science Foundation grant number 0726909,

JSPS-RFBR contract number 09-02-92114, Grant-in-Aid for Scientific Research (S), MEXT Kakenhi on Quantum Cybernetics and Funding Program for Innovative R&D on S&T (FIRST). JQY acknowledges partial support from the National Natural Science Foundation of China under grant number 10625416, the National Basic Research Program of China under grant number 2009CB929300 and the ISTCP under grant number 2008DFA01930. X-FC acknowledges support from the National Natural Science Foundation of China under grant number 10904126 and the Fujian Province Natural Science Foundation under grant number 2009J05014.

## Appendix A. Two unitary transformations on two baths

This appendix offers a detailed derivation of the transformed Hamiltonian (2) from the original Hamiltonian (1) through unitary transformations. To deal with the anti-rotating terms in equation (1), we apply the first canonical transformation to the Hamiltonian $H$

$$\tilde{H} = \exp(S_1) H \exp(-S_1), \tag{A.1}$$

with

$$S_1 = \sum_k \frac{g_{k,1}}{\omega_{k,1}} \xi_{k,1} (a_{k,1}^\dagger - a_{k,1}) \sigma_x. \tag{A.2}$$

Here a $k$-dependent variable $\xi_{k1} = \omega_{k,1}/(\omega_{k,1} + \eta_1 \Delta)$ is introduced into the transformation. The transformed Hamiltonian $\tilde{H}$ can be decomposed into three parts:

$$\tilde{H} = \tilde{H}_0 + \tilde{H}_1 + \tilde{H}_2, \tag{A.3}$$

with

$$\tilde{H}_0 = \frac{1}{2}\eta_1 \Delta \sigma_z + \sum_{k,i} \omega_{k,i} a_{k,i}^\dagger a_{k,i} - \sum_k \frac{g_{k,1}^2}{\omega_{k,1}} \xi_{k,1} (2 - \xi_{k,1}), \tag{A.4}$$

$$\tilde{H}_1 = \sum_k 2\eta_1 \Delta \frac{g_{k,1}\xi_{k,1}}{\omega_{k,1}} (a_{k,1}^\dagger \sigma_- + a_{k,1}\sigma_+) + \sum_k g_{k,2} (a_{k,2}^\dagger + a_{k,2}) \sigma_x, \tag{A.5}$$

$$\begin{aligned} \tilde{H}_2 = {} & \frac{1}{2}\Delta\sigma_z \left[ \cosh\left( \sum_k \frac{2g_{k,1}}{\omega_{k,1}} \xi_k (a_{k,1}^\dagger - a_{k,1}) \right) - \eta_1 \right] \\ & + \mathrm{i}\frac{\Delta}{2}\sigma_y \left[ \sinh\left( \sum_k \frac{2g_{k,1}}{\omega_{k,1}} \xi_k (a_{k,1}^\dagger - a_{k,1}) \right) - \eta_1 \sum_k \frac{2g_{k,1}}{\omega_{k,1}} \xi_k (a_{k,1}^\dagger - a_{k,1}) \right], \end{aligned} \tag{A.6}$$

where $\eta_1 = \exp[-\sum_k (2g_{k,1})^2 {\xi_{k,1}}^2 / 2\omega_{k,1}^2]$. The parameter $\eta_1$ is determined by $\langle 0_{k,1}|\tilde{H}_2|0_{k,1}\rangle$. Then $\eta_1$ contains the contribution from zero-boson transition and is regarded as a renormalization factor of the qubit energy spacing $\Delta$. $\tilde{H}_1$ contains the terms of single-boson transition, whose contribution to the physical quantities is of order $\mathcal{O}(g_{k,1}^2)$. The terms in $\tilde{H}_2$ are related to the double- and multiboson nondiagonal transitions such as $a_{k,1}^\dagger a_{k',1}^\dagger$ and $a_{k,1}a_{k',1}$, whose contributions to the physical quantities are of order $\mathcal{O}(g_{k,1}^4)$. In the zero-temperature case,

the contribution from these multiboson nondiagonal transitions may be dropped safely. So, in the following calculation, we dropped all the higher-order terms in $\tilde{H}_2$. Thus, the effective transformed Hamiltonian can be derived as

$$\tilde{H} \approx \frac{1}{2}\eta_1 \Delta\sigma_z + \sum_{k,i} \omega_{k,i} a_{k,i}^{\dagger} a_{k,i} + \sum_k g_{k,2}(a_{k,2}^{\dagger} + a_{k,2})\sigma_x + \sum_k \tilde{g}_{k,1}(a_{k,1}^{\dagger}\sigma_- + a_{k,1}^{-}\sigma_+), \tag{A.7}$$

with $\tilde{g}_{k,1} = 2\eta_1 \Delta g_{k,1}/(\omega_{k,1} + \eta_1 \Delta)$.

Then, we apply a second similar transformation to the transformed Hamiltonian $\tilde{H}$: $H' = \exp(S_2)\tilde{H}\exp(-S_2)$, with $S_2 = \sum_k \frac{g_{k,2}}{\omega_{k,2}} \xi_{k,2}(a_{k,2}^{\dagger} - a_{k,2})\sigma_x$ and $\xi_{k,2} = \omega_{k,2}/(\omega_{k,2} + \eta_2 \Delta)$, and obtain

$$H' = H_0' + H_1' + H_2', \tag{A.8}$$

with

$$H_0' = \frac{1}{2}\eta_1\eta_2 \Delta\sigma_z + \sum_{k,i} \omega_{k,i} a_{k,i}^{\dagger} a_{k,i} - \sum_{k,i} \frac{g_{k,i}^2}{\omega_{k,i}} \xi_{k,i}(2 - \xi_{k,i}), \tag{A.9}$$

$$H_1' = \sum_{k,i} 2\eta_i \Delta \frac{g_{k,i}\xi_{k,i}}{\omega_{k,i}}(a_{k,i}^{\dagger}\sigma_- + a_{k,i}\sigma_+), \tag{A.10}$$

$$H_2' = \frac{1}{2}\Delta\sigma_z \left[\cosh\left(\sum_k \frac{2g_{k,2}}{\omega_{k,2}} \xi_{k,2}(a_{k,2}^{\dagger} - a_{k,2})\right) - \eta_2\right] + \mathrm{i}\frac{\Delta}{2}\sigma_y \left[\sinh\left(\sum_k \frac{2g_{k,2}}{\omega_{k,2}} \xi_{k,2}(a_{k,2}^{\dagger} - a_{k,2})\right) - \eta_2 \sum_k \frac{2g_{k,2}}{\omega_{k,2}} \xi_{k,2}(a_{k,2}^{\dagger} - a_{k,2})\right], \tag{A.11}$$

where $\eta_2 = \exp[-\sum_k (2g_{k,2})^2 \xi_{k,2}{}^2/2\omega_{k,2}^2]$. This $\eta_2$ is one more renormalization factor of $\Delta$ from the second bath. Because the constant term $\sum_{k,i} g_{k,i}^2 \xi_{k,i}(2 - \xi_{k,i})/\omega_{k,i}$ has no effect on the dynamics evolution, we neglect it. As in the same approximation of the first transformation, we drop the higher-order terms in $H_2'$ and the mixed effect of two baths, whose contributions to the physical quantities are $\mathcal{O}(g_{k,2}^4)$ or $\mathcal{O}(g_{k,1}^2 g_{k,2}^2)$. At last, we obtain the transformed Hamiltonian $H'$

$$H' \approx \frac{1}{2}\eta_1\eta_2 \Delta\sigma_z + \sum_{k,i} \omega_{k,i} a_{k,i}^{\dagger} a_{k,i} + \sum_{k,i} \tilde{g}_{k,i}(a_{k,i}^{\dagger}\sigma_- + a_{k,i}^{-}\sigma_+), \tag{A.12}$$

with $\tilde{g}_{k,i} = 2\eta_i \Delta g_{k,i}/(\omega_{k,i} + \eta_i \Delta)$.

## Appendix B. Solution of the equation of motion for the density matrix

This appendix offers detailed calculations for solving the master equation in equation (18). We use the basis $|1\rangle = |\downarrow\rangle$ and $|2\rangle = |\uparrow\rangle$, where $\sigma_z|\downarrow\rangle = |\downarrow\rangle$, $\sigma_z|\uparrow\rangle = -|\uparrow\rangle$, to define the reduced density matrices of the qubit. Using the Laplace transform

$$\tilde{\rho}(p) = \mathcal{L}[\rho(t)] = \int_0^{\infty} \mathrm{d}t \rho(t) \exp(-pt) \tag{B.1}$$

and the convolution theorem

$$\mathcal{L}\left[\int_0^t \mathrm{d}t' f_1(t') f_2(t-t')\right] = \mathcal{L}\left[f_1(t)\right]\mathcal{L}\left[f_2(t)\right], \tag{B.2}$$

the master equation (18) for the qubit system can be solved as

$$p\tilde{\rho}_S^{I'}(p) - \rho_S'(0) = -A_-\sigma_+\sigma_-\tilde{\rho}_S^{I'}(p) + (A_+ + A_-)\,\sigma_-\tilde{\rho}_S^{I'}(p)\sigma_+ - A_+\tilde{\rho}_S^{I'}(p)\sigma_+\sigma_-, \tag{B.3}$$

where

$$A_\pm = \sum_{k,i}^{2} \tilde{g}_{k,i}^2 \Big/ [p \pm \mathrm{i}(\omega_{k,i} - \eta\,\Delta)]. \tag{B.4}$$

Equation (18) is a Lyapunov matrix equation.

The Kronecker product property in matrix theory shows that

$$\mathrm{Vec}(M_1\rho M_2) = M_1 \otimes M_2^{\mathrm{T}}\,\mathrm{Vec}(\rho), \tag{B.5}$$

where $\mathrm{Vec}(\rho)$ represents the vector expanding matrix $\rho$ along rows, and the superscript T denotes the transpose of the matrix. We expand the matrix equation in equation (B.3) into vectors along rows

$$U(p)\,\mathrm{Vec}[\tilde{\rho}_S^{I'}(p)] = \mathrm{Vec}[\rho_S'(0)], \tag{B.6}$$

where

$$U(p) = pI_4 + A_+ I_2 \otimes (\sigma_+\sigma_-)^{\mathrm{T}} - (A_- + A_+)\sigma_- \otimes \sigma_+^{\mathrm{T}} + A_-(\sigma_+\sigma_-) \otimes I_2, \tag{B.7}$$

where $I_n$ is the $n \times n$ identity matrix. Thus, the $2 \times 2$ matrix equation (B.3) is transformed to the $4 \times 4$ vector equation (B.6). The solution of equation (B.6) can be formally written as

$$\mathrm{Vec}\left[\tilde{\rho}_S^{I'}(p)\right] = U(p)^{-1}\,\mathrm{Vec}[\rho_S'(0)], \tag{B.8}$$

with

$$U(p)^{-1} = \begin{pmatrix} \frac{1}{p+A_++A_-} & 0 & 0 & 0 \\ 0 & \frac{1}{p+A_-} & 0 & 0 \\ 0 & 0 & \frac{1}{p+A_+} & 0 \\ \frac{1}{p} - \frac{1}{p+A_++A_-} & 0 & 0 & \frac{1}{p} \end{pmatrix}. \tag{B.9}$$

Using the inverse Laplace transform

$$\alpha(t) = \mathcal{L}^{-1}[\tilde{\alpha}(p)] = \frac{1}{2\pi\mathrm{i}}\int_{\sigma-\mathrm{i}\infty}^{\sigma+\mathrm{i}\infty} \mathrm{d}p\;\tilde{\alpha}(p)\exp(pt), \tag{B.10}$$

we obtain

$$\mathrm{Vec}[\rho_S^{I'}(t)] = \mathcal{L}^{-1}U(p)^{-1}\,\mathrm{Vec}[\rho_S'(0)]. \tag{B.11}$$

Then, $\rho_S^{I'}(t)$ is given by

$$\rho_S^{I'}(t) = \mathcal{L}^{-1}\begin{pmatrix} \left[\frac{\rho_{11}(0)}{p+A_++A_-}\right] & \left[\frac{\rho_{12}(0)}{p+A_+}\right] \\ \left[\frac{\rho_{21}(0)}{p+A_-}\right] & \left[\frac{\rho_{11}(0)}{p} - \frac{\rho_{11}(0)}{p+A_++A_-} + \frac{\rho_{22}(0)}{p}\right] \end{pmatrix}. \tag{B.12}$$

Below we calculate the inverse Laplace transform $\mathcal{L}^{-1}(\frac{1}{p+A_\pm})$ and $\mathcal{L}^{-1}(\frac{1}{p+A_++A_-})$. From equation (B.10), we have

$$\mathcal{L}^{-1}\left(\frac{1}{p+A_-}\right) = \frac{1}{2\pi \mathrm{i}}\int_{\sigma-\mathrm{i}\infty}^{\sigma+\mathrm{i}\infty} \frac{\exp(pt)}{p+\sum_{k,i}\tilde{g}_{k,i}^2/[p-\mathrm{i}(\omega_{k,i}-\eta\,\Delta)]}\,\mathrm{d}p. \tag{B.13}$$

With $p$ replaced by $\mathrm{i}\omega + 0^+$ [37], the above expression becomes

$$\mathcal{L}^{-1}\left(\frac{1}{p+A_-}\right) = \frac{1}{2\pi \mathrm{i}}\int_{-\infty}^{+\infty} \frac{\exp(\mathrm{i}\omega t)}{\omega-\sum_{k,i}\tilde{g}_{k,i}^2/[(\omega+\eta\,\Delta)-\omega_{k,i}-\mathrm{i}0^+]}\,\mathrm{d}\omega. \tag{B.14}$$

For the term $\sum_k \tilde{g}_{k,i}^2/(\omega-\omega_{k,i}-\mathrm{i}0^+)$, we denote the real and imaginary parts as $R_i(\omega)$ and $\Gamma_i(\omega)$, where $i=1$ for the intrinsic bath and $i=2$ for the cavity bath. Explicitly, we can write

$$\begin{aligned} R_i(\omega) &= \wp\left(\sum_k \frac{\tilde{g}_{k,1}^2}{\omega-\omega_{k,1}}\right) \\ &= \wp\left[\int_0^\infty \mathrm{d}\omega' \left(\frac{2\eta_1\,\Delta}{\omega'+\eta_1\Delta}\right)^2 \frac{J_1(\omega')}{(\omega-\omega')}\right], \end{aligned} \tag{B.15}$$

and

$$\begin{aligned} \Gamma_i(\omega) &= \pi\sum_k \tilde{g}_{k,i}^2\,\delta(\omega-\omega_{k,1}) \\ &= \pi\left(\frac{2\eta_i\,\Delta}{\omega+\eta_i\,\Delta}\right)^2 J_i(\omega), \end{aligned} \tag{B.16}$$

where $\wp$ stands for the Cauchy principal value. Let $R(\omega)=R_1(\omega)+R_2(\omega)$ and $\Gamma(\omega)=\Gamma_1(\omega)+\Gamma_2(\omega)$; then we have

$$\mathcal{L}^{-1}\left(\frac{1}{p+A_-}\right) = \frac{1}{2\pi \mathrm{i}}\int_{-\infty}^{+\infty} \frac{\exp(\mathrm{i}\omega t)}{\omega-R(\omega+\eta\,\Delta)-\mathrm{i}\Gamma(\omega+\eta\,\Delta)}\mathrm{d}\omega. \tag{B.17}$$

Similarly, $\mathcal{L}^{-1}\frac{1}{p+A_+}$ and $\mathcal{L}^{-1}\frac{1}{p+A_++A_-}$ can also be derived as

$$\mathcal{L}^{-1}\left(\frac{1}{p+A_+}\right) = \left[\mathcal{L}^{-1}\left(\frac{1}{p+A_-}\right)\right]^* \tag{B.18}$$

and

$$\begin{aligned} &\mathcal{L}^{-1}\left(\frac{1}{p+A_++A_-}\right) \\ &\quad = \frac{1}{2\pi \mathrm{i}}\int_{-\infty}^{+\infty} \frac{\exp(\mathrm{i}\omega t)}{\omega-R(\omega+\Delta\eta)+R(\Delta\eta-\omega)-\mathrm{i}\,[\Gamma(\omega+\Delta\eta)+\Gamma(\Delta\eta-\omega)]}\mathrm{d}\omega. \end{aligned} \tag{B.19}$$

## Appendix C. Derivation of equation (25)

Below, we prove that equation (25) is established through solving the Schrödinger equation beyond the RWA in the transformed Hamiltonian (2). Since the total excitation number operator of the qubit–cavity system, $N=\sum_{k,i} a_{k,i}^{\dagger}a_{k,i}+(1+\sigma_z)/2$, in the transformed Hamiltonian is a conserved observable, i.e. $[N, H']=0$, it is reasonable to restrict our discussion to the single-particle excitation subspace. A general state in this subspace can be written as

$$|\Phi(t)\rangle=\chi(t)\,|s2\rangle\prod_{k}\left|0_{k,1}0_{k,2}\right\rangle+\sum_{k,i}\beta_{k,i}(t)\,|s1\rangle\prod_{k}\left|0_{k,\bar{i}}1_{k,i}\right\rangle, \tag{C.1}$$

where the state $\left|0_{k,\bar{i}}1_{k,i}\right\rangle$ means either a cavity bath or a qubit intrinsic bath with one quantum excitation. Substituting $|\Phi(t)\rangle$ into the Schrödinger equation, we have

$$\mathrm{i}\frac{\mathrm{d}\chi(t)}{\mathrm{d}t}=\frac{\eta\,\Delta}{2}\chi(t)+\sum_{k,i}\tilde{g}_{k,i}^{2}\beta_{k,i}(t), \tag{C.2}$$

$$\mathrm{i}\frac{\mathrm{d}\beta_{k,i}(t)}{\mathrm{d}t}=\left(\omega_{k,i}-\frac{\eta\,\Delta}{2}\right)\beta_{k,i}(t)+\sum_{k,i}\tilde{g}_{k,i}^{2}\chi(t). \tag{C.3}$$

Applying the transformation

$$\chi(t)=\tilde{\chi}(t)\exp\left(-\mathrm{i}\frac{\eta\,\Delta}{2}t\right), \tag{C.4}$$

$$\beta_{k,i}(t)=\tilde{\beta}_{k,i}(t)\exp\left[-\mathrm{i}\left(\omega_{k,i}-\frac{\eta\,\Delta}{2}\right)t\right], \tag{C.5}$$

equations (C.2) and (C.3) are simplified to

$$\frac{\mathrm{d}\tilde{\chi}(t)}{\mathrm{d}t}=-\mathrm{i}\sum_{k,i}\tilde{g}_{k,i}^{2}\tilde{\beta}_{k,i}(t)\exp\left[-\mathrm{i}(\omega_{k,i}-\eta\,\Delta)t\right], \tag{C.6}$$

$$\frac{\mathrm{d}\tilde{\beta}_{k,i}(t)}{\mathrm{d}t}=-\mathrm{i}\tilde{g}_{k,i}^{2}\tilde{\chi}(t)\exp\left[\mathrm{i}(\omega_{k,i}-\eta\,\Delta)t\right]. \tag{C.7}$$

Integrating equation (C.7) and substituting it into equation (C.6), we obtain

$$\frac{\mathrm{d}\tilde{\chi}(t)}{\mathrm{d}t}=-\int_{0}^{t}\sum_{k,i}\tilde{g}_{k,i}^{2}\exp[-\mathrm{i}(\omega_{k,i}-\eta\,\Delta)(t-t')]\tilde{\chi}(t')\mathrm{d}t'. \tag{C.8}$$

This integro-differential equation (C.8) is solved exactly by Laplace transformation:

$$\overline{\tilde{\chi}(p)}=\frac{1}{p+A_{+}}=\frac{\tilde{\chi}(0)}{p+\sum_{k,i}\tilde{g}_{k,i}^{2}/[p-\mathrm{i}(\eta\,\Delta-\omega_{k,i})]}. \tag{C.9}$$

When the initial state is an excited state, $|\psi'(0)\rangle=|\uparrow\rangle\otimes\prod_{k}\left|0_{k,1},0_{k,2}\right\rangle$, i.e. $\tilde{\chi}(0)=1$. Applying the inverse Laplace transformation, we obtain

$$\tilde{\chi}(t)=\left(\mathcal{L}^{-1}\frac{1}{p+A_{+}}\right)_{t}. \tag{C.10}$$

Combining equation (B.18), the dynamic evolution of the density matrix element $\rho'_{11}$ is expressed as

$$\begin{aligned}\rho'_{11}(t) &= \chi^*(t) \times \chi(t) \\ &= \left(\mathcal{L}^{-1}\frac{1}{p+A_+}\right)_t \times \left(\mathcal{L}^{-1}\frac{1}{p+A_-}\right)_t . \end{aligned} \tag{C.11}$$

## References


[1] Khitrova G, Gibbs H M, Kira M, Koch S W and Scherer A 2006 *Nat. Phys.* **2** 81
[2] Gunter G *et al* 2009 *Nature* **458** 178
[3] You J Q and Nori F 2005 *Phys. Today* **58** 42
You J Q and Nori F 2011 *Nature* **474** 589
[4] Schoelkopf R J and Girvin S M 2008 *Nature* **451** 664
[5] Ashhab S and Nori F 2010 *Phys. Rev.* A **81** 042311
[6] Reuther G M *et al* 2010 *Phys. Rev.* B **81** 144510
[7] You J Q and Nori F 2003 *Phys. Rev.* B **68** 064509
[8] Blais A, Huang R S, Wallraff A, Girvin S M and Schoelkopf R J 2004 *Phys. Rev.* A **69** 062320
[9] Lev Bishop S, Chow J M, Koch J, Houck A A, Devoret M H, Thuneberg E, Girvin S M and Schoelkopf R J 2009 *Nat. Phys.* **5** 105
[10] Fink J M *et al* 2010 arXiv:1003.1161v1
[11] Thompson R J, Rempe G and Kimble H J 1992 *Phys. Rev. Lett.* **68** 1132
[12] Reithmaier J P, Sek G, Löffler A, Hofmann C, Kuhn S, Reitzenstein S, Keldysh L V, Kulakovskii V D, Reinecke T L and Forchel A 2004 *Nature* **432** 197
[13] Yoshie T, Scherer A, Hendrickson J, Khitrova G, Gibbs H M, Rupper G, Ell C, Shchekin O B and Deppe D G 2004 *Nature* **432** 200
[14] Wallraff A, Schuster D I, Blais A, Frunzio L, Huang R-S, Majer J, Kumar S, Girvin S M and Schoelkopf R J 2004 *Nature* **431** 162
[15] Bloch F and Siegert A 1940 *Phys. Rev.* **57** 522
[16] Shirley J H 1965 *Phys. Rev.* **138** B979
[17] Wei C, Holmstromk S A, Sellarsy M J, Mansony N B and Ficek Z 1997 *J. Phys. B: At. Mol. Opt. Phys.* **30** 2735
[18] Cao X, You J Q, Zheng H, Kofman A G and Nori F 2010 *Phys. Rev.* A **82** 022119
[19] De Liberato S, Ciuti C and Carusotto I 2007 *Phys. Rev. Lett.* **98** 103602
[20] Zueco D, Reuther G M, Kohler S and Hanggi P 2009 *Phys. Rev.* A **80** 033846
[21] Niemczyk T 2010 *Nat. Phys.* **6** 772
[22] Johansson J R, Johansson G, Wilson C M and Nori F 2009 *Phys. Rev. Lett.* **103** 147003
Johansson J R, Johansson G, Wilson C M and Nori F 2010 *Phys. Rev.* A **82** 052509
[23] De Liberato S, Gerace D, Carusotto I and Ciuti C 2009 *Phys. Rev.* A **80** 053810
[24] Uchiyama C, Aihara M, Saeki M and Miyashita S 2009 *Phys. Rev.* E **80** 021128
[25] Ciuti C and Carusotto I 2006 *Phys. Rev.* A **74** 033811
[26] Devoret M, Girvin S and Schoelkopf R 2007 *Ann. Phys.* **16** 767
[27] McDermott R 2009 *IEEE Trans. Appl. Supercond.* **19** 2
[28] Mazzola L, Maniscalco S, Piilo J, Suominen K-A and Garraway B M 2009 *Phys. Rev.* A **79** 042302
[29] Mintert F, Carvalho A R R, Kuś M and Buchleitner A 2005 *Phys. Rep.* **415** 207
[30] Scully M O and Zubairy M S 1997 *Quantum Optics* (Cambridge: Cambridge University Press)
Ficek Z and Tanaś R 2002 *Phys. Rep.* **372** 369
[31] Carmichael H J 2002 *Statistical Methods in Quantum Optics 1* (New York: Springer)
Carmichael H J, Brecha R J, Raizen M G, Kimble H J and Rice P R 1989 *Phys. Rev.* A **40** 5516

[32] Rzażewski K, Wodkiewicz K and Żakowicz W 1975 *Phys. Rev. Lett.* **35** 432
[33] Auffèves A, Besga B, Gérard J-M and Poizat J-P 2008 *Phys. Rev.* A **77** 063833
[34] Carmichael H J and Walls D F 1973 *J. Phys. A: Math. Gen.* **6** 1552
Carmichael H J and Walls D F 1974 *Phys. Rev.* A **9** 2686
[35] Cresser J 1992 *J. Mod. Opt.* **39** 2187
[36] Schuster D I *et al* 2007 *Nature* **445** 515
[37] Mahan G D 1990 *Many-Particle Physics* (New York: World Scientific)